Eur. Phys. J. Plus (2021) 136:408
https://doi.org/10.1140/epjp/s13360-021-01423-x

THE EUROPEAN PHYSICAL JOURNAL PLUS

Regular Article

Effects of healthy aging on electrical activity of the brain during motor tasks characterized with wavelets

A.N. Pavlov[1,2,a], **E.N. Pitsik**[3], **G.A. Guyo**[1], **N.S. Frolov**[3], **V.V. Grubov**[3], **O.N. Pavlova**[1], **Z. Wang**[4], **A.E. Hramov**[2,3,5]

[1] Saratov State University, Astrakhanskaya Str. 83, Saratov, Russia 410012
[2] Regional Scientific and Educational Mathematical Center "Mathematics of Future Technologies", 23 Gagarina Avenue, Nizhny Novgorod, Russia 603950
[3] Neuroscience and Cognitive Technology Laboratory, Center for Technologies in Robotics and Mechatronics Components, Innopolis University, Universitetskaya Str. 1, Innopolis, The Republic of Tatarstan, Russia 420500
[4] Northwestern Polytechnical University, 27 West Youyi Road, Beilin District, Xi'an 710072, Shaanxi, China
[5] Saratov State Medical University, Bolshaya Kazachya Str. 112, Saratov, Russia 410012

Received: 6 November 2020 / Accepted: 10 April 2021

Abstract Age-related changes in the brain's electrical activity can be caused by healthy aging and brain disorders. The ability to detect such phenomena from an electroencephalogram (EEG) is important to identify diseases' latent stages. These changes appear in the brain's background electrical activity, but the performance of cognitive or motor tasks can cause more significant signs of impairments in brain dynamics. Here, we analyze the features of multichannel EEGs in groups of healthy elderly and younger adults during hand clenching and apply two wavelet-based methods to reveal distinctions that arise with age, namely multiresolution analysis using the discrete wavelet transform, and multifractal formalism, which involves extracting the skeleton of the continuous wavelet transform. With the first method, we demonstrate that inter-group differences are established at rest and during the performance of motor tasks. With the second method, we also find similar distinctions, although the number of suitable channels and their distribution can differ. We conclude that characterization of age-related differences depends on the wavelet-based method used for EEG processing.

1 Introduction

Aging causes numerous chronic changes in the human body, which include impairments of biological and physiological processes leading to various disabilities. In addition to the increased susceptibility and frequency of diseases associated with a decrease in the functions of different organs, changes occur in social and psychological processes, and they also significantly reduce the quality of daily life. Aging affects brain dynamics, and many studies focus on pathological conditions such as Alzheimer's disease or dementia. Over the past decades, significant progress has been reached in understanding the physiological mecha-

[a] e-mail: pavlov.alexeyn@gmail.com (corresponding author)

nisms responsible for these disorders [1–4]. However, the ability to distinguish latent stages of brain diseases from mild disorders associated with healthy aging is still unclear. Understanding such differences can offer effective biomarkers for identifying early disease stages and risk factors. Healthy aging affects neurochemical, structural and functional changes in the brain [5], causing impaired cognitive and motor function that results in a slower reaction time, decreased motor control, coordination [6], etc. According to recent studies [7–9], elderly adults may use additional areas of the brain during physical activity to compensate for the corresponding changes in brain dynamics [10,11]. The latter explains expected differences between younger and elderly adults in the performance of motor tasks and in the resting state activity. In particular, young adults tend to use the efficient and fast mechanism of motor working memory [12].

Many researchers have addressed age-related changes in cognitive or motor function using various signal processing tools and multichannel EEGs to link the revealed phenomena to specific areas of the brain [13–18]. For a deeper understanding of the results, they can be associated with EEG rhythms and related electrical activity in the frequency bands of θ (4–8 Hz), α (8–12 Hz), β (15–30 Hz), and other waves. For this purpose, time-frequency processing of EEG is performed using windowed Fourier transform, wavelet transform [19–21], or Hilbert-Huang transform [22], which allow characterizing the signal features in selected ranges of scales. The application of machine learning algorithms can also improve the characterization of age-related impairments [23,24]. Other approaches consider abnormalities in the complexity of EEG to identify different neurological disorders [25,26]. This is a vast research topic with many ways to quantify complexity. In particular, it was established that healthy aging tends to increase the complexity of brain activity reflected in EEG recordings, and the relationship between the complexity measures and age was revealed [27]. Changes in complexity can serve as a marker for the development of neurodegenerative disorders [25,26]. Besides the complexity of brain activity, age-related distinctions appear in the long-range power-law correlations of EEG data [28].

The performance of signal processing tools may differ when examining rapid responses during short-term motor or cognitive tasks, and the limitations of methods for short and non-stationary data can strongly affect the results, as opposed to considering resting states. In this regard, the ability to reliably characterize age-related effects may depend on the method used and the appropriate choice of the EEG channel. In the current study, we apply fairly versatile signal processing tools such as the multiresolution analysis using the DWT [20,29,30] and the wavelet-based multifractal formalism [31–33]. Both of these tools decompose datasets using soliton-like functions that serve as band-pass filters. Wavelets with several vanishing moments enable ignoring polynomial trends that typically appear during transition processes between different states, e.g., the state of rest and the execution of motor tasks. An important measure in the first approach is the dependence of the standard deviation of decomposition coefficients on the time scale [29]. The second approach is well adapted for the statistical analysis of inhomogeneous processes and describes the complex structure of experimental data in terms of the singularity spectrum. The key numerical quantities associated with such a spectrum are the mean Hölder (or Hurst) exponent, which characterizes the correlation features, and the spectrum width being a measure of the signal inhomogeneity (complexity). Here we demonstrate the efficiency of both tools in studying age-related changes in the EEG and their features in the detection of such changes.

The work is organized as follows. Section 2 describes experimental fine motor tasks in groups of elderly and younger adults and briefly discusses EEG processing techniques. Section 3 contains key findings on age-related differences in multichannel EEGs and a discussion

of the methods performances in quantifying distinctions between the two groups of subjects. In Sect. 4, we briefly summarize the concluding remarks.

2 Experiments and methods

2.1 Participants and experimental procedures

The experiments were carried out with twenty healthy right-handed volunteers, divided into two groups: 10 young adults aged 26.1±5.15 (mean±SD), and 10 elderly adults aged 65.0±5.69. All subjects had no medical history of neural pathological conditions (brain tumors, trauma, stroke) and signed written informed consents before participating in experimental procedures. The experiments were performed in accordance with the protocol approved by the local ethics committee of the Innopolis University (Kazan, Russia) and the Declaration of Helsinki.

All volunteers were asked to sit on a chair with the hands placed comfortably on the table in front of them, palms up. The background EEG was recorded in a relaxed state (5 minutes, eyes open). The active phase of the experiment consisted of 60 repetitions of a fine motor task. Each task included clenching the hand into a fist after the beep and unclenching after the repeated beep. Such fine motor task was performed by the non-dominant hand (left hand, LH, 30 trials), controlled by short beeps (0.3 s), and by the dominant hand (right hand, RH, 30 trials), carried out after longer beeps (0.75 s). The order of movements (LH or RH) was selected randomly. The total duration of the experimental procedure was about 15 minutes per participant. For further data analysis, we extracted 12-second recordings associated with each individual trial, which included a baseline EEG (2 s), clenching the hand and holding it until a repeated beep (4–5 s), unclenching the hand and pause before the next task (6–8 s).

2.2 Data recording and preprocessing

We recorded multichannel EEG according to the "10–10" registration scheme with 31 channels (O2, O1, P4, P3, C4, C3, F4, F3, Fp2, Fp1, P8, P7, T8, T7, F8, F7, Oz, Pz, Cz, Fz, Fpz, FT7, FC3, FCz, FC4, FT8, TP7, CP3, CPz, CP4, TP8), two reference electrodes A1 and A2 on the earlobes and a ground electrode N above the forehead. We used Ag/AgCl cup adhesive electrodes placed on the "Tien–20" paste (Weaver and Company, Denver, CO, USA). To improve the skin's conductivity and decrease its resistance, we applied NuPrep abrasive gel from the same manufacturer. After installing the electrodes, the impedance was controlled in the 2/5 kΩ interval during experimental procedures. The "Encephalan-EEG-19/26" electroencephalograph (Medicom MTD company, Taganrog, Russian Federation) had a registration certificate of the Federal Service for Supervision in Health Care No. FCP 2007/00124 dated 07.11.2014 and a European certificate CE 538571 of the British Standards Institute. The EEG was acquired with a sampling rate of 250 Hz, filtered using a 50 Hz notch filter and a Butterworth bandpass filter (with cut-off frequencies of 1 Hz and 100 Hz). Artifacts produced by heartbeats and blinking of eyes were extracted with independent component analysis [34]. In the course of visual inspection, some segments were removed in which the latter approach did not provide adequate suppression of artifacts. For further analysis, we selected half of the cleanest segments (15 motor tasks per hand). Data preprocessing was carried out using the MNE package for Python 3.7 (ver. 0.20.0) [35]. Selected EEG segments are available online [36].

2.3 Multiresolution analysis

The multiresolution analysis uses an iterative pyramidal decomposition of a signal over two sets of orthonormal mirror filters, low-pass filters $\varphi_{j,k}(t)$, and high-pass filters $\psi_{j,k}(t)$, constructed from scaling function $\varphi(t)$ and mother wavelet $\psi(t)$ by dilations with the scale factor 2^j and integer translations k [12]

$$\varphi_{j,k}(t) = 2^{-j/2}\varphi(2^{-j}t - k), \qquad \psi_{j,k}(t) = 2^{-j/2}\psi(2^{-j}t - k). \tag{1}$$

Each time scale associated with some value of j contains an independent set of information in the form of the approximation coefficients estimated by expansion over scaling functions, and detail coefficients computed by expansion over wavelets. The transitions between scales are described by the following equations:

$$\varphi(t) = \sqrt{2}\sum_{k=0}^{2M-1} h_k\varphi(2t - k), \qquad \psi(t) = \sqrt{2}\sum_{k=0}^{2M-1} g_k\psi(2t - k), \tag{2}$$

where $g_k = (-1)^k h_{2M-k-1}$, and $2M$ is the number of coefficients h_k or g_k that define the filters. These coefficients are estimated numerically from the general properties of $\varphi(t)$ and $\psi(t)$ as solutions to some functional equations containing rescaling and translations. For the simplest wavelet from the Daubechies family (D^4), h_k have analytical expressions, but for higher-order Daubechies wavelets they are given as numerical values estimated with the required accuracy [19]. The number of vanishing moments of $\varphi(t)$ is equal to M. Larger M is associated with the better regularity properties, i.e. the smoother functions, however, this is not always the optimal choice, and usually a trade-off is made between the support length and regularity. The D^8 wavelet is often considered as such a compromise.

A function $x(t) \in L^2(R)$ at the selected resolution level j_n can be expanded as follows

$$x(t) = \sum_k s_{j_n,k}\varphi_{j_n,k}(t) + \sum_{j\le j_n}\sum_k d_{j,k}\psi_{j,k}(t). \tag{3}$$

This expansion includes the computation of approximation ($s_{j,k}$) and detail ($d_{j,k}$) coefficients at each stage (resolution level j), permutation of the vector of coefficients for separating s- and d-coefficients and selecting only the s-coefficients for the next stage. A fast computation algorithm using both direct and inverse transformations is discussed in the book [37].

The sequence of coefficients varies between scales and throughout the entire signal in the case of nonstationary datasets. A simple measure of this variability is the standard deviation of $d_{j,k}$ as a function of the scale j:

$$\sigma(j) = \sqrt{\frac{1}{J}\sum_{k=0}^{J-1}\left[d_{j,k} - \langle d_{j,k}\rangle\right]^2}, \tag{4}$$

where J is the number of detail coefficients at the scale j. The $\sigma(j)$ dependence quantifies fluctuations associated with different frequency bands. It is often used in physiological studies to diagnose distinctions between normal and pathological dynamics [29].

2.4 Multifractal formalism

The multifractal formalism, revisited using the continuous wavelet transform, was proposed in [31] and characterizes a signal in terms of the singularity spectrum $D(h)$. The latter is

computed based on the partition functions constructed from the wavelet transform modulus maxima (WTMM). Thus, the method includes several stages, namely:

(1) Estimation of the wavelet-transform coefficients of the distribution function $f(x)$

$$W(x_0, a) = \frac{1}{a} \int_{-\infty}^{\infty} f(x) \psi \left(\frac{x - x_0}{a} \right) \mathrm{d}x, \tag{5}$$

where ψ is the basic wavelet, a is the scale parameter. Unlike many other approaches, the results of the WTMM method do not depend on ψ (theoretically, when we do not take into account the restrictions of the datasets under study, the presence of noise, etc.). For this reason, fairly simple real-valued functions such the MHAT or WAVE wavelets are chosen as ψ. If x_0 is a singularity point, then $|W(x_0, a)|$ increases as $x \to x_0$, and a power-law dependence appears

$$W(x_0, a) \sim a^{h(x_0)}, \tag{6}$$

which is quantified by the Hölder exponent $h(x_0)$. For non-singular points, the wavelet coefficients behave differently, and, therefore, each singularity gives a line of maxima of $|W(x_0, a)|$.

(2) Extracting all lines of local maxima of $|W(x, a)|$ (skeleton lines). Although $h(x_0)$ can be computed from Eq. (6), this is a rather unstable procedure due to the influence of neighboring singularities.

(3) Construction of the partition function

$$Z(q, a) = \sum_{l \in L(a)} |W(x_l(a), a)|^q \sim a^{\tau(q)}, \tag{7}$$

where $L(a)$ is the complete set of skeleton lines existing at the a scale, $x_l(a)$ is the position of the maximum associated with the l line. A more stable algorithm based on partition functions is discussed in the original paper [32]. Typically, the partition function exhibits a power-law behavior with a scaling exponent $\tau(q)$

$$Z(q, a) \sim a^{\tau(q)}. \tag{8}$$

(4) Estimation of the Hölder exponents $h(q)$ and the singularity spectrum $D(h)$ using the Legendre transform

$$h(q) = \frac{\mathrm{d}\tau(q)}{\mathrm{d}q}, \qquad D(h) = qh - \tau(q). \tag{9}$$

For positive q, the $D(h)$ spectrum characterizes strong singularities in the data sets; and for negative q it quantifies the features of weak singularities. The value D is the Hausdorff dimension of a data subset with the Hölder exponent h. Two simple quantities can be introduced to characterize the singularity spectrum: the mean Hölder exponent $H = h(0)$, associated with the more frequently occurring singularity, and the width Δ of $D(h)$, which defines the degree of inhomogeneity (multifractality). The value Δ is a measure of the complexity of the function $f(x)$.

3 Results and discussion

3.1 Multiresolution analysis

For data processing, we selected 3 parts from 12-second recordings related to each task ($N = 2^9$ samples per part), which correspond to the baseline EEG (part 1), clenching the hand into a fist (part 2) and unclenching the fist (part 3). To exclude the influence of individual motor tasks, statistical analysis was carried out for each volunteer (separately for LH and RH) by averaging $\sigma(j)$ dependencies over 15 repetitive tasks. The DWT-based multiresolution analysis with Daubechies wavelet D^8 shows an increase in $\sigma(j)$ with a scale j for every part, that is consistent with the results of other studies of physiological time series, e.g., [29,38]. Inter-group distinctions appear at $j \geq 4$. Figure 1 illustrates an example of the results obtained for the measure σ for $j = 5$ on the plane (σ_3, σ_1), where the index denotes the analyzed part (in this example, 3 and 1). Here the channels $C3$ and $C4$ are chosen, which were discussed in the previous study [28] and provided reliable inter-group separation. Our results show that σ values generally decrease with age, and this effect is observed both at rest and during motor activity. Consideration of part 2 provides a qualitatively similar behavior, which indicates that age-related distinctions can be identified in different parts of the experimental recordings. Visual inspection of Fig. 1 suggests that dominant hand motor activity may better discriminate between the elderly and younger adults.

Further, we computed $\sigma(j)$ for all channels and available scales and compared the possibilities of revealing significant age-related distinctions based on the Student's t-test ($p < 0.05$). Table 1 summarizes the estimations and shows that inter-group distinctions improve when the scale changes from $j = 4$ to $j = 5$. With a further increase in the j scale, no obvious improvement is observed: the distinctions may be better at rest ($j = 7$ compared to $j = 5$),

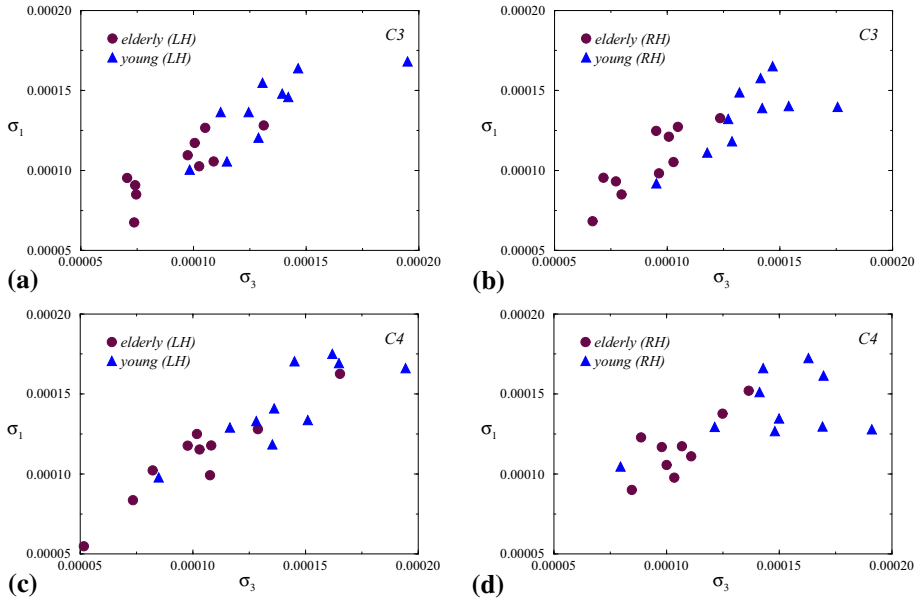

Fig. 1 Multiresolution analysis of elderly and younger adults during rest (σ_1) and hand unclenching (σ_3) for $j = 5$: **a** C3 channel, LH, **b** C3 channel, RH, **c** C4 channel, LH, and **d** C4 channel, RH

Table 1 The number of EEG channels with significant age-related distinctions, determined using the DWT-based multiresolution analysis according to the Student's t-test ($p < 0.05$)

Scale	Movement	Part 1 (rest)	Part 2 (clenching)	Part 3 (unclenching)
$j = 4$	LH	10	9	13
	RH	12	13	10
$j = 5$	LH	22	21	19
	RH	24	21	23
$j = 6$	LH	21	20	15
	RH	25	22	20
$j = 7$	LH	24	13	15
	RH	25	24	18

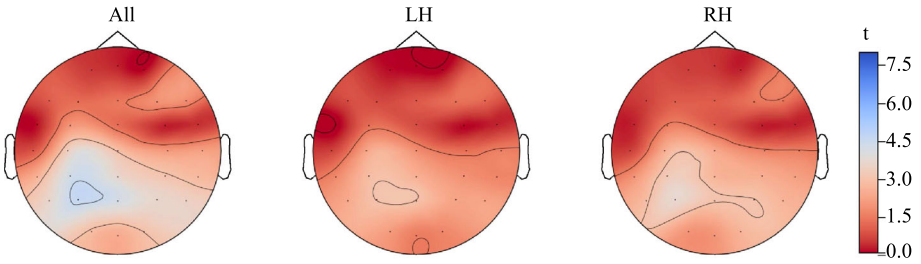

Fig. 2 Distributions of t-values (multiresolution analysis, $j = 4$) for all movements, LH- and RH-movements

but the opposite effect is observed with motor activity. Some variations in the number of channels are caused by the t-values being close to the critical level (t_c) associated with $p = 0.05$, and variations near t_c may affect the estimated number of channels. Resolution levels $j = 5$ and $j = 6$ seem to be preferable.

The distribution of t-values depending on the position of the electrodes makes it possible to identify areas of the brain in which age-related distinctions in electrical activity are well pronounced. Figure 2 illustrates such a distribution for the scale $j = 4$ including the results for all movements (both hands), LH- and RH-movements. Although there are fewer channels for inter-group separation (Table 1, $j = 4$) compared to other levels of resolution, we can associate these changes with the parietal area, and confirm pronounced distinctions in the central and occipital areas of the brain as well. For larger scales, the number of channels providing significant age-related distinctions increases, but the distribution of t-values is fairly similar (see Fig. 3).

3.2 Multifractal formalism

The WTMM approach separates two groups based on the mean Hölder exponent and the degree of multifractality. Unlike some studies, where the multifractal formalism showed advantages and outperformed other wavelet-based tools, here we observed a decrease (compared to the DWT-based multiresolution analysis) in the number of EEG-channels with a reliable identification of age-related distinctions (Table 2). Despite this circumstance, the inter-group separation can be carried out both from background measurements (5–9 channels, depending on the measure used) and during motor activity (5–12 channels), i.e., the

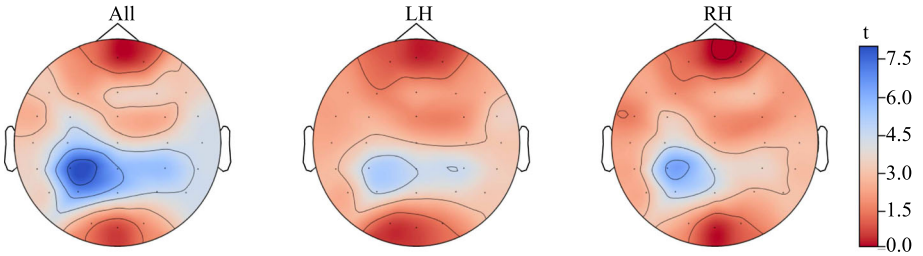

Fig. 3 Distributions of t-values (multiresolution analysis, $j = 5$)

Table 2 The number of EEG channels with significant age-related distinctions when using the WTMM method according to the Student's t-test ($p < 0.05$)

Measure	Movement	Part 1 (rest)	Part 2 (clenching)	Part 3 (unclenching)
H	LH	9	5	6
	RH	7	9	8
Δ	LH	6	6	4
	RH	5	12	7

results are comparable for these states. Several features of the results should be mentioned. For dominant hand (RH) movements, the distinctions are stronger with hand clenching (9 versus 5 channels for H, and 12 versus 6 channels for Δ), while for non-dominant hand (LH) movements, the number of suitable channels may even decrease when performing motor tasks compared to rest (5 versus 9 channels for H). On average, inter-group distinctions are better observed at rest for the H-measure and while hand clenching for the Δ-measure. We hypothesize that the decrease in the number of suitable channels within the wavelet-based multifractal formalism may be due to limited data sets (512 samples) that are small enough to cover a wide range of scales when studying the scaling laws for the partition functions for each scale and, therefore, essential computational errors can occur that affect the shape of the singularity spectrum. The multiresolution analysis is a simpler technique that does not require power-law approximations at the varying range of scales. Investigations using another rather simple approach, namely, the detrended fluctuation analysis [39–41], also demonstrated a better ability to diagnose age-related effects in EEG signals compared to WTMM [28].

The distribution of t-values depending on the position of the electrodes is illustrated in Figs. 4 (mean Hölder exponent) and 5 (width of the singularity spectrum). The strongest distinctions appear for recordings from TP8, FT8, FT7 channels (H-measure) and T3, T4, Oz, F4, F7, C4, C3 channels (Δ-measure). Comparison with the results of multiresolution analysis (Figs. 2, 3) and an analogous study performed using DFA [28] leads to the conclusion that the selection of an appropriate channel may differ depending the approach to signal processing. On the one hand, this can be caused by restricted statistics (10 subjects per group) and short data sets (512 samples) that possess an inhomogeneous structure during motor activity. The latter can affect the performances of methods, leading to finite-samples effects. On the other hand, significant inter-group differences are observed for many EEG-channels for different areas of the brain (for some channels, $p < 0.001$). This suggests that characterization of age-related differences may depend on the measure applied to EEG recordings.

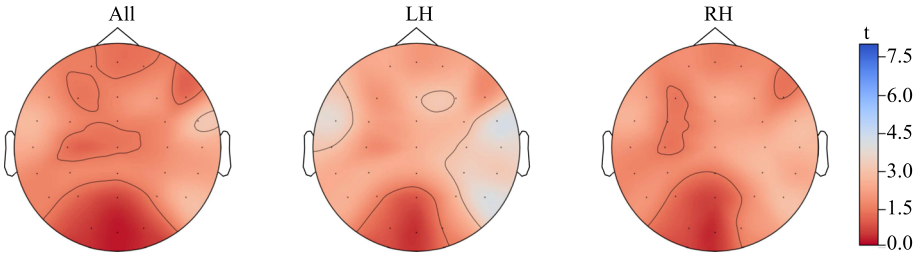

Fig. 4 Distributions of t-values (WTMM, mean Hölder exponent)

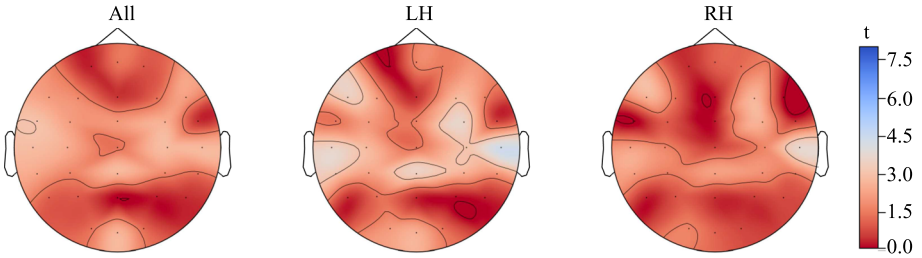

Fig. 5 Distributions of t-values (WTMM, width of the singularity spectrum)

Thus, our study shows that processing of multichannel EEGs makes it possible to use wavelet-based tools to recognize age-related changes in brain electrical activity. Depending on the quantitative measure, the strongest differences can be revealed at rest or during motor activity.

4 Conclusion

Knowledge of age-related changes in brain dynamics is important for identifying early stages of disorders, the physiological signs of which are similar to healthy aging. In the current study, we have applied two wavelet-based methods, the multiresolution analysis with DWT and the WTMM-approach, to reveal age-related distinctions in groups of healthy elderly and younger adults. The first method establishes inter-group differences with standard deviations of detail coefficients in non-overlapping ranges of scales that can be identified both at rest and during fine motor tasks. These differences are often stronger for motor tasks carried out by the dominant hand. The second method also performs inter-group separation, although the number of suitable channels is smaller, and their distribution differs from the results of multiresolution analysis. We suppose that the decrease in the number of suitable channels can be explained by a rather small number of samples during motor tasks. We also concluded that wavelet-based approaches are effective for studying age-related differences, although their characterization depends on the signal processing technique.

This work was supported by the Russian Foundation for Basic Research (Grant 19-52-55001) in the part of experimental studies and numerical analysis. ANP acknowledges the support by the grant of the Government of the Russian Federation No. 075-15-2019-1885 in the part of theoretical analysis of the restrictions of the multifractal formalism in relation to EEG data.

References

1. R.M. Steketee, R. Meijboom, M. de Groot, E.E. Bron, W.J. Niessen, A. van der Lugt, J.C. van Swieten, M. Smits, Neurobiol. Aging **43**, 119 (2016)
2. M. Yu, A.A. Gouw, A. Hillebrand, B.M. Tijms, C.J. Stam, E.C. van Straaten, Y.A. Pijnenburg, Neurobiol. Aging **42**, 150 (2016)
3. E. Yu, Z. Liao, D. Mao, Q. Zhang, G. Ji, Y. Li, Z. Ding, Curr. Alzheimer Res. **14**, 628 (2017)
4. E.R. Lindemer, D.N. Greve, B.R. Fischl, J.C. Augustinack, D.H. Salat, NeuroImage Clin. **14**, 156 (2017)
5. Q. Lin, M.D. Rosenberg, K. Yoo, T.W. Hsu, T.P. O'Connell, M.M. Chun, Front. Aging Neurosci. **10**, 94 (2018)
6. C. Maes, J. Gooijers, J.J.O. de Xivry, S.P. Swinnen, M.P. Boisgontier, Neurosci. Biobehav. Rev. **75**, 234 (2017)
7. S. Heuninckx, N. Wenderoth, S.P. Swinnen, J. Neurosci. **28**, 91 (2008)
8. J. Langan, S. Peltier, J. Bo, B.W. Fling, R.C. Welsh, R.D. Seidler, Front. Syst. Neurosci. **4**, 17 (2010)
9. M. Berchicci, G. Lucci, C. Pesce, D. Spinelli, F. Di Russo, Neuroimage **62**, 1750 (2012)
10. J. Fernandez-Ruiz, A. Peltsch, N. Alahyane, D.C. Brien, B.C. Coe, A. Garcia, D.P. Munoz, Neuroimage **165**, 92 (2018)
11. N.S. Ward, Ageing Res. Rev. **5**, 239 (2006)
12. N.S. Frolov, E.N. Pitsik, V.A. Maksimenko, V.V. Grubov, A.R. Kiselev, Z. Wang, A.E. Hramov, PLoS ONE **15**(9), e0233942 (2020)
13. J. Dushanova, M. Christov, Adv. Med. Sci. **59**, 61 (2014)
14. F. Ferreri, A. Guerra, L. Vollero, D. Ponzo, S. Maatta, E. Mervaala, G. Iannello, V. Di Lazzaro, Neuroscience **357**, 255 (2017)
15. P.A. Reuter-Lorenz, D.C. Park, Neuropsychol. Rev. **24**, 355 (2014)
16. T. Bardouille, L. Bailey, CamCAN Group. Neuroimage **193**, 25 (2019)
17. K. Cassady, H. Gagnon, P. Lalwani, M. Simmonite, B. Foerster, D. Park, S.J. Peltier, M. Petrou, S.F. Taylor, D.H. Weissman, R.D. Seidler, T.A. Polk, Neuroimage **186**, 234 (2018)
18. C.-H. Cheng, M.-Y. Lin, S.-H. Yang, Front. Aging Neurosci. **10**, 53 (2018)
19. I. Daubechies, *Ten Lectures on Wavelets*. Society for Industrial and Applied Mathematics, 1992
20. A.N. Pavlov, A.E. Hramov, A.A. Koronovskii, E.Y. Sitnikova, V.A. Makarov, A.A. Ovchinnikov, Phys. Usp. **55**, 845 (2012)
21. A.E. Hramov, A.A. Koronovskii, V.A. Makarov, A.N. Pavlov, E. Sitnikova, *Wavelets in Neuroscience* (Springer, Berlin, 2015)
22. N.E. Huang, Z. Shen, S.R. Long, M.C. Wu, H.H. Shih, Q. Zheng, N.-C. Yen, C.C. Tung, H.H. Liu, Proc. R. Soc. A **454**, 903 (1998)
23. V.A. Maksimenko, S.A. Kurkin, E.N. Pitsik, V.Y. Musatov, A.E. Runnova, T.Y. Efremova, A.E. Hramov, A.N. Pisarchik, Complexity **2018**, 9385947 (2018)
24. P. Chholak, G. Niso, V.A. Maksimenko, S.A. Kurkin, N.S. Frolov, E.N. Pitsik, A.E. Hramov, A.N. Pisarchik, Sci. Rep. **9**, 9838 (2019)
25. S. Nobukawa, T. Yamanishi, H. Nishimura, Y. Wada, M. Kikuchi, T. Takahashi, Cogn. Neurodyn. **13**, 1 (2019)
26. D. Labate, F. La Foresta, I. Palamara, G. Morabito, A. Bramanti, Z. Zhang, F.C. Morabito, in *Recent Advances of Neural Network Models and Applications*. Springer, 2014, p. 163
27. N. Scheel, E. Franke, T.F. Münte, A Madany Mamlouk. Front. Hum. Neurosci. **12**, 451 (2018)
28. A.N. Pavlov, E.N. Pitsik, N.S. Frolov, A. Badarin, O.N. Pavlova, A.E. Hramov, Sensors **20**, 5843 (2020)
29. S. Thurner, M.C. Feurstein, M.C. Teich, Phys. Rev. Lett. **80**, 1544 (1998)
30. V.A. Maksimenko, A. Pavlov, A.E. Runnova, V. Nedaivozov, V. Grubov, A. Koronovskii, S.V. Pchelintseva, E. Pitsik, A.N. Pisarchik, A.E. Hramov, Nonlinear Dyn. **91**, 12803 (2018)
31. J.-F. Muzy, E. Bacry, A. Arneodo, Phys. Rev. Lett. **67**, 3515 (1991)
32. J.-F. Muzy, E. Bacry, A. Arneodo, Phys. Rev. E **47**, 875 (1993)
33. A. Arneodo, E. Bacry, J.F. Muzy, Phys. A **213**, 232 (1995)
34. A. Hyvärinen, E. Oja, Neural Netw. **13**, 411 (2000)
35. A. Gramfort, M. Luessi, E. Larson, D.A. Engemann, D. Strohmeier, C. Brodbeck, R. Goj, M. Jas, T. Brooks, L. Parkkonen, M. Hämäläinen, Front. Neurosci. **7**, 267 (2013)
36. N. Frolov, E. Pitsik, V. Grubov, A. Kiselev, V. Maksimenko, A. Hramov, https://figshare.com/articles/EEG_dataset_for_the_analysis_of_age-related_changes_in_motor-related_cortical_activity_during_a_series_of_fine_motor_tasks_performance/12301181/1
37. W.H. Press, S.A. Teukolsky, W.T. Vetterling, B.P. Flannery, *Numerical Recipes, 3rd Edition: The Art of Scientific Computing* (Cambridge University Press, Cambridge, 2007)

38. A.N. Pavlov, D.S. Grishina, A.E. Runnova, V.A. Maksimenko, O.N. Pavlova, N.V. Shchukovsky, A.E. Hramov, J. Kurths, Chaos Solitons Fractals **126**, 230 (2019)
39. C.-K. Peng, S. Havlin, H.E. Stanley, A.L. Goldberger, Chaos **5**, 82 (1995)
40. R.M. Bryce, K.B. Sprague, Sci. Rep. **2**, 315 (2012)
41. Y.H. Shao, G.F. Gu, Z.Q. Jiang, W.X. Zhou, D. Sornette, Sci. Rep. **2**, 835 (2012)